Initial Conditions of the Universe that Permitted the Growth of Structures

Xintong Xie

E-mail: xxt.christine@gmail.com

Accepted for publication: 2023
Published Date: October 2023

Abstract

While the Big Bang theory has been adopted by many, further research ponders on the Cosmic Microwave Background (CMB) which is the relic radiation from the Big Bang that records much relevant and crucial information. Not only does CMB reveal traits of later formations of cosmological structures, but it is also closely related to how our universe started and consequently behaved. In this paper, I will delve into further studies regarding the CMB of our current universe, as well as providing similar studies of a hypothetical universe for comparison.

Keywords: Cosmology, inflation, Cosmic Microwave Background, polarisation, anisotropy, B-mode, power spectrum.

1. Introduction

The Cosmic Microwave Background (CMB) is relic radiation from the Big Bang and serves as an important tool for exploring the initial conditions of the universe. Microscopic scales of temperature and polarisation fluctuations of the CMB are evidence of early cosmic events (e.g. [1, 2]). CMB temperature and polarisation measurements have allowed physicists to constrain the age, geometry, and distribution of matter in the universe, while also providing evidence for dark energy (e.g. [2, 3, 4]). Future measurements of the CMB will target constraints on inflationary gravitational waves [5].

The inflationary theory predicts a rapid exponential expansion of the early universe which would have caused quantum fluctuations in a small, hot, dense universe to evolve into the large-scale structure (galaxy clusters) we see today [5]. This expansion would have also formed gravitational waves, which have a unique signature in the CMB polarisation maps, in particular, the B-mode polarisation signal [4].

In this research, NASA simulated CMB data will be used to understand the measurement process and filtering techniques of the CMB (fourier transform, power spectrum, autocorrelation). I will then simulate my own version of the universe to see how that affects the measurement of the CMB by comparing the B-mode power spectrum between NASA's data and my data. This will build an intuition of how parameters affect the initial conditions of the universe, which I will discuss in my paper. NASA simulated data will also be used to compare with experimental data from the Atacama Cosmology Telescope (ACT). This is to examine the differences between theoretical predictions of the CMB temperature power spectrum with actual measured data.

2. Inflation

Under current levels of study of the universe, the Big Bang theory is the most widely-accepted in terms of explaining how the universe came into place (e.g. [1, 2, 3, 4]). Prior to even the Big Bang, the universe was this singularity where everything was causally connected [5]. It then underwent exponential expansion, according to the inflationary theory, where the universe expanded at speed much greater than today's speed of light, such that everything appeared causally disconnected. It has been deduced that the universe increased in size by at least 10^{26} in less than 10^{-32}s during the Big Bang [6]. Inflation stops and regular expansion (known as Hubble expansion) starts when the universe was just macroscopic [6]. The universe then had about the same amount of expansion in the subsequent 13.7 billion years than that of inflation [5].

The inflationary theory is most recognized because it explains three unexplained problems in the universe.

Namely, these are the monopole problem, the horizon problem, and the flatness problem [7].

2.1 Monopole Problem

According to the previous Big Bang theory where the universe was theorised to expand on a steady rate, magnetic monopoles were predicted to exist in the universe though they have yet to be detected [8], contradicting the old predictions. The theory of inflation provides an explanation. As the universe expanded exponentially, the density of magnetic monopoles decreased significantly to the point where none can be detected from our point of observation [8].

2.2 Horizon Problem

For any two photons in the universe with distance greater than the product of speed of light times age of the universe, they theoretically are impossible to have been in contact with each other, according to the previous Big Bang theory [9]. This is because these 2 CMB photons would have to travel for time longer than the age of the universe to get to each other.

However, studies on CMB radiation shows that such two photons are actually causally connected due to their same temperature [10]. Inflationary theory predicts this as it tells us that the universe used to be a very small, hot, and dense point prior to the Big Bang, thus everything was once causally connected with another [7].

2.3 Flatness Problem

Through calculations on the CMB background, the universe is found to be very flat [11]. This indicates that if the universe expanded at a steady rate, its initial state must be very near to perfect flatness, which is of low probability. Inflation solves this problem because as the universe expands exponentially, all points can be seen as the centre of expansion [12]. Even if the initial stage of the universe was curved, it would appear flat on a very small scale after expansion, which is why today's universe appears very flat.

As inflation solves the above three discrepancies in the universe, it is critical to determine whether this event occurred in the early universe. A direct detection of the inflationary event can only be studied through the Cosmic Microwave Background (CMB) (e.g. [1, 2, 3, 4]).

3. Formation of the CMB

The Cosmic Microwave Background (CMB) can be considered as leftover radiation from the Big Bang. It has a nearly uniform temperature of 2.7 Kelvin [10] and behaves very close to a blackbody [13], which is an idealised physical body that absorbs all incident electromagnetic waves.

The CMB was formed as a result of the Recombination epoch, which is around 370 000 years after the Big Bang, when charged electrons and protons first became bound to form electrically neutral hydrogen atoms [14]. Prior to the Recombination epoch (also referred to as the decoupling epoch), the universe was a hot, dense, plasma of photons, leptons, quarks, and subsequently protons [15]. Stable neutral atoms were unable to form due to the high temperatures. Free electrons scattered off photons, a process known as Thomson scattering, causing photons to be unable to travel long distances [14]. The Universe was thus opaque.

At 370 000 years after the Big Bang, the temperature of the universe cooled to 3000 Kelvin. The epoch of Recombination starts here [14]. Photon-electron interaction in this epoch decreased as the lower temperature no longer supported such interactions [14]. Formation of neutral hydrogen atoms become energetically favoured as hydrogen atoms formed with electrons at high energy states [14]. These electrons later transited to low energy states by emitting photons, a process known as photon decoupling [14]. Decoupled photons no longer hindered by the electrons were able to travel freely in space, becoming what is now known as the CMB, and thus the universe became transparent.

As the universe expanded, it continued to decrease in temperature. As a result, the CMB photons that were released at 3000K lowered in energy to about 2.7K today, meaning the photons released from decoupling now peak in the microwave region of the electromagnetic spectrum. The places where these photons last interacted with the electrons is known as the surface of last scattering [16].

4. Critical Features of the CMB

The radiation spectrum of CMB fits the black body spectrum to very high precision, while other objects in the universe generally follow the power laws [13]. The black body is an idealised physical body that absorbs all incident electromagnetic radiation [17]. Figure 1 shows an example of a black body radiation spectrum.

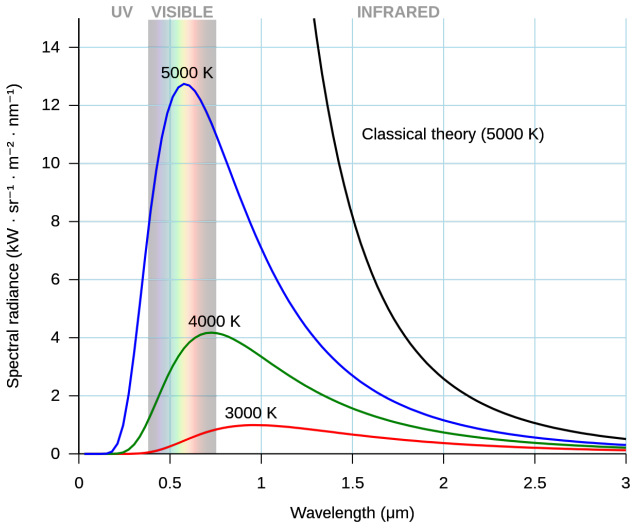

[Figure 1. Blackbody radiation. Image from[18]]

The CMB power spectrum is obtained from measurements of a range of parameters, among which are roughly 8 parameters that are sufficiently independent of each other and of enough significance to be discussed separately below in Figure 2.

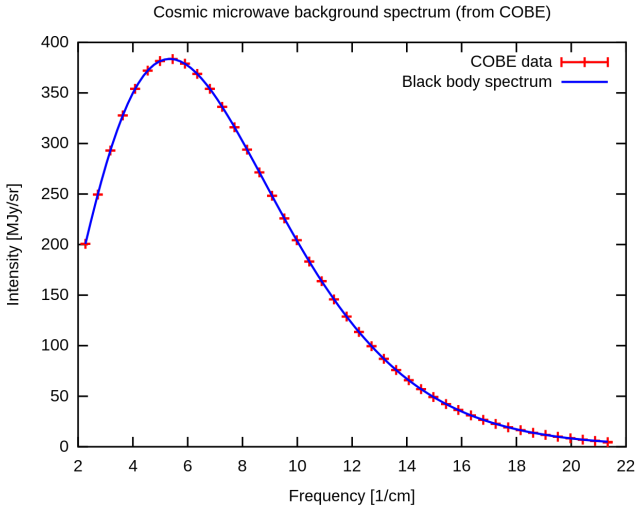

[Figure 2. Level of agreement of CMB data and the blackbody spectrum, measured by the FIRAS instrument on the COBE. Image from[13]]

One factor that describes the primordial universe is the energy scale of inflation (r) which gives information of the energy level of the very early universe [19]. Another important factor is the equation-of-state parameter (w) that is the ratio of the pressure of the dark energy to its energy density [19]. It indicates how much dark energy was present in the early universe [19].

Optical depth (τ) from the epoch of reionization also tells us when, how, and what the first stars in the galaxy looked like, giving us information on early cosmological structure formations [19]. The rest 5 factors characterise the present universe. This includes the rate of expansion of the universe (Hubble constant), curvature of the universe (Ωk), and the density of the major three components of the universe respectively. That is, baryon (normal matter including radiation) density, matter (dark matter) density, and dark energy density [19].

Another important characteristic of present day CMB is that it falls into the microwave part of the spectrum, as is implied by its name. This occurs due to a phenomenon known as redshift [20]. As the universe expands, the speed of light remains constant, causing the wavelength of the CMB photons to be stretched as it moves away from our point of view [20]. The frequency of these photons decreases through time and falls into the microwave spectrum today. This process can be considered as the Doppler shift of light.

4.1 Fourier Decomposition

Fourier decomposition breaks the density fluctuations of the universe into a number of component sine waves of different frequencies [21].

At times when the universe was still opaque, dark matter would lump together over time, making the dark matter fluctuations bigger and bigger since they are only affected by gravity [22]. Acoustic oscillations moving at the then speed of sound, which was around 57% of the speed of light, occurred in the photon-baryon fluid [22]. This resulted in a number of waves with the same speed but different frequencies and wavelengths. For waves that have higher frequency in space, their faster rate of change in densities also corresponds to some higher frequency waves in time.

As the universe expanded, cooled, and became transparent, the speed of sound decreased enormously [22]. Photons were also no longer trapped with the baryons [14]. When we observe the CMB today, what we see is a snapshot of the particular moments on these sine waves at the time of recombination [23]. The sine waves with longer wavelength correspond to the larger angular scales or lower order multipoles part of the power spectrum [23]. Very few fluctuations are observed in this region. The large-scale nature of these waves means that there are few of them, which makes data interpretation harder.

4.2 Discovery of CMB

The CMB was first predicted in 1948 by American cosmologist Ralph Apher [24]. Several years later in 1964, the CMB was accidentally found by Arno Penzias and Robert Wilson [25], and later identified by Robert Dicke's team [26]. Among all spacecraft missions to study the CMB, there were three key initial ones, naming COBE, WMAP, and Planck.

COBE was sent out by NASA from 1989 to 1993. It detected that CMB is at around 2.73 Kelvin [27]. It observed small temperature fluctuations on the order of 1 in 100000 across the CMB [27]. It also produced the first space-based full-sky map of the CMB [27], which confirmed the Big Bang theory predictions and showed hints of cosmic structures not seen before.

WMAP was sent out by NASA from 2001 to 2010. The aim of this space mission was to study the small fluctuations across the CMB in detail. It discovered that the small temperature fluctuations of CMB reflected the slightly higher or lower densities in the primordial universe [28], which later grew into large-scale structures under the effect of gravity [28]. In 2003, it produced the first picture that indicated the universe to be 13.7 billion years old [28], while previous discoveries gave the number 13.8. Scientists later studied the very early stage of inflation, universe's lumpiness and other properties, leading to discovery of asymmetry in average temperatures in both hemispheres of the sky and a bigger cold spot than expected [28]. WMAP's data determined the proportions of the fundamental constituents of the universe, and have been used to establish the standard model of cosmology.

Planck was later sent out by ESA (and was significantly contributed to by NASA) from 2009 to 2013 aiming to refine the standard model of cosmology. It observes the universe at wavelengths between 0.3 mm and 11.1 mm, which are the far-infrared, microwave, and high frequency radio domains [29]. It covered a wider frequency range and had higher sensitivity, able to measure temperature variations of a few millionths of a degree, thus showing the tiny fluctuations in greater detail and precision. Its data confirmed the previous discoveries of asymmetry and the cold spot [29]. It also produced the highest precision picture of CMB yet from satellites [29]. Using its data, scientists later uncovered that fluctuations in the CMB at large angular scales did not match predictions.

Figure 3 below shows the comparison between precision of CMB data collected by the three journeys respectively.

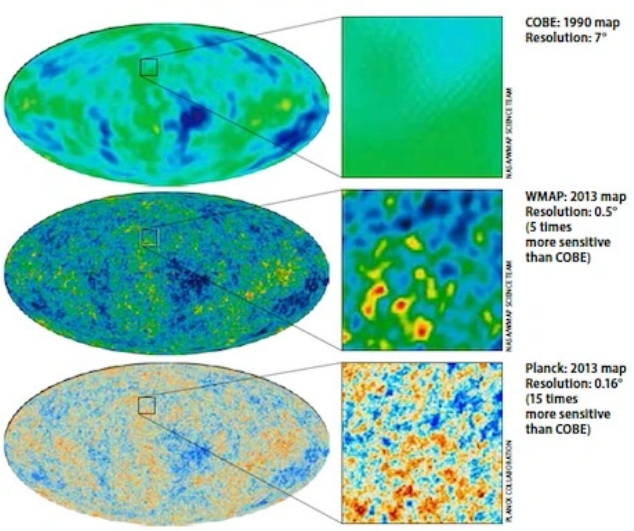

[Figure 3. Close-up views of the CMB from the 3 experiments. Image from[30]]

5. Anisotropies of the CMB

It is previously stated that the CMB has a nearly uniform temperature of 2.73 Kelvin [10]. However, temperature variations of a few microkelvin still exist across the CMB [31]. Such temperature differences in turn lead to density differences [31], of which the process will be elaborated later. Together, these two differences are called the anisotropies of the CMB. To put in more scientific terms, CMB anisotropies refers to its directional dependency [31], which means that the CMB has different properties in different regions.

CMB anisotropies are categorised into two types—the primary anisotropy due to effects that occurred at the surface of last scattering and before, and the secondary (also referred to as the late-time anisotropy) due to effects that occurred between the surface of last scattering and the observer (i.e., now) [32].

Primary anisotropies were principally determined by two effects that occurred in the early universe. The first is the baryonic acoustic oscillations [22]. In the early universe, gravity acted to bring the baryons together. As the baryons move towards each other, they heat up, causing an increase in pressure which pulls them apart. The combination of these two forces drove the baryon acoustic oscillations. It can be viewed as the tendency to create overdense anisotropies versus the tendency to erase it [22]. The second is diffusion damping, also referred to as silk damping or collisionless damping [33]. Photon diffusion damping is a process that reduced density anisotropies in the early universe. During the recombination epoch, photons travelled freely from hot regions to cold regions, dragging along electrons and thus protons, equalising the temperatures of these regions [33].

On the other hand, secondary anisotropies were influenced by two effects that occurred between reionization (an epoch of the universe that occurs just before the formation of stars and galaxies) and our observations of the CMB [34]. The first is the Sunyaev-Zeldovich effect where the hot, dense materials at the centres of galaxy clusters scatter the microwave photons from CMB up to higher frequencies [34]. This is why when clusters are observed in microwaves, decrements appear at the position of the clusters. The second is the Sachs-Wolfe effect [35]. This effect explains how variations in densities in the CMB lead to temperature fluctuations [35].

In general, CMB has a uniform temperature of about 2.725 Kelvin [10]. However, tiny temperature fluctuations exist because of gravitational redshift [35]. At the surface of last scattering, there is a Sachs-Wolfe effect [35]. Due to fluctuations in the density of the universe and the fact that matter curves space, higher density leads to more curvature of space. At places where space is more curved, light loses more energy to escape the gravitational potential wall. The photons thus become gravitationally redshifted, and hence the CMB spectrum appears to be uneven [35].

Between the surface of last scattering and the Earth, there exists the integrated Sachs-Wolfe effect [36], which states that the gravitational effects of travelling into a certain region do not necessarily equal the gravitational effects of travelling out of the same region later on [36]. This effect occurs due to the presence of dark energy [36]. When photons enter a region of overdensity, they gain energy as they travel in. The gravitational potential well then becomes stretched and shallower as photons travel through due to the effect of dark energy. When photons leave the region, they lose a smaller amount of energy. The overall gain in energy leads to relatively higher temperatures surrounding these regions of overdensity, which leads to the overdense areas having relatively cooler temperatures [36]. Vice versa for regions of underdensity. To conclude, overdensities lead to cold spots and underdensities lead to hot spots in the CMB.

6. Polarisation of the CMB

CMB polarisation is a phenomenon where the electric field of the CMB radiation oscillates more in one direction than another [37]. It occurs at the level of a few microkelvin [37].

The polarisation of the CMB is caused by a process known as quadrupolar distribution through Thomson scattering, a form of elastic scattering among particles. Quadrupolar temperature variations occur as a result of electron interactions in areas of hotter spots in the photon-baryon plasma in the early universe with greater amplitude of radiation leading to linearly polarised CMB light [38]. Quadrupolar patterns exist because of the flow of the primordial plasma [38], the material that the CMB was released from during decoupling.

There are two types of CMB polarisation—B-modes and E-modes [31]. E-modes arose mainly from Thomson scattering [31]. They are analogous to electric fields, meaning they are scalar fields that arise from density perturbations in the universe and have vanishing curls in terms of mathematical notations [39]. E-modes are sourced from scalar perturbations in the early universe (i.e. tiny changes in the density of matter in the early, smaller, hotter universe [39]); therefore, they help us understand the evolution of structure formation in our universe [39]. Along with the temperature of the CMB, E-mode polarisation has been detected and measured in various CMB experiments to good precision.

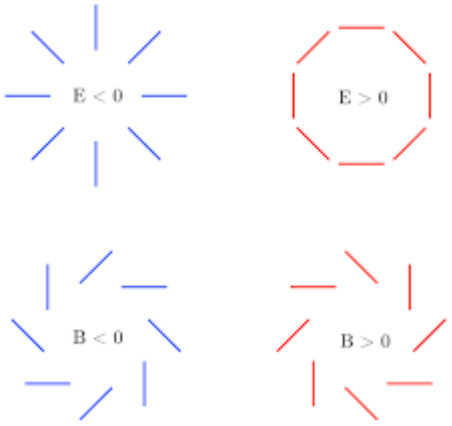

[Figure 4. E and B-mode dashes. Image from [40]]

However, B-modes are theorised to arise from gravitational waves generated from cosmic inflation [39], and have not yet been detected but are a large motivating factor for current and future CMB experiments.

Gravitational waves are cosmic ripples in space-time that are caused by energetic processes [41]. They travel at the speed of light and carry information about their source. Theory suggests that during inflation, gravitational waves were produced in enormous intensities, and remnants of its effect should appear as a very faint background of gravitational waves in the universe [42]. Since this background is too faint to be directly detected, researchers today point to the CMB to find evidence of a specific polarisation signal (B-modes) that only inflation could have caused. The amplitude of such a signal, in turn, describes the energy scale of inflation, r [19]. B-mode signals, however, are difficult to detect even within the CMB because the degree of foreground contamination is unknown, and weak gravitational lensing signals mix strong E-modes signals with B-modes [43].

Both E- and B-mode features are seen in the Fourier modes that are created from polarisation in the CMB, thus the analogous coined electromagnetic terms for E- and B-modes. In terms of forms, pure E-modes have polarisation parallel or perpendicular to the direction of the wave vector, while pure B-modes have polarisation rotated to 45° about the wave direction [40]. CMB polarisation can thus be viewed as the superposition of B-modes and E-modes.

7. Angular Power Spectrum of the CMB

As is stated above, the radiation spectrum of the CMB fits the black-body spectrum very well while other objects in the universe generally follow the power laws [13]. This characteristic is used to obtain the CMB anisotropy map by subtracting the effects of other cosmic objects through space.

In spherical harmonics, any signal which appears in the sky with equal intensity at every location is referred to as a monopole [44]. Ell ("l") is a dimensionless index associated with the number of spatial oscillations in the θ direction [44], where the relationship between ell and θ is given by the equation $l = 180° / \theta$. Ell is inversely related to the angular separation—the lower the l value, the larger the angular scale, where an angular scale of 1 degree on the sky is the size of the moon. For the monopole, l equals 0. Number of nodes equals l plus 1. The monopole image therefore has a single constant intensity.

In Planck data of the CMB, the value of l goes up to 2500 (e.g. [1, 29]). Using spherical harmonics, CMB anisotropy maps can be turned into angular power spectra.

Below are theoretical power spectra plots for CMB temperature and polarisation. Note that, though it does not show in the figure below, measurements for temperature and E-modes have been made but not at the highest ell values, and a B-mode measurement from inflation has not yet been detected. The goal for next-generation CMB experiments is to reach those high ell values as well as reach higher instrument sensitivities to make a measurement of the B-mode gravitational wave signal.

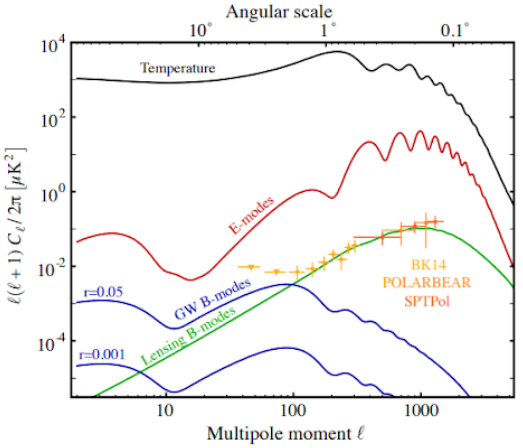

[Figure 5. Theoretical predictions of the respective power spectra. Plot from [45]]

The figure above has the TT power spectrum (black), EE power spectrum (red), the two BB power spectra (blue), and the power spectrum of E-mode lensing into B-mode (yellow being the data measured, green being the theoretical curve). The TT (black) and EE (red) curves are related to each other because they both provide information of structure formation in the universe [46].

When there is a peak in the temperature curve, there is a correlating trough in the E-mode polarisation curve, as is shown in Figure 5. This is because as baryons are brought together by gravity during the process of baryonic acoustic oscillations, they first heat up, then get pulled apart by the increase in pressure [22]. This indicates that higher levels of E-mode polarisation are directly related to overdense regions. Meanwhile, the integrated Sachs-Wolfe effect [36] tells us that overdensities generally have cooler temperatures.

The two B-mode power spectra indicate the range of possible actual B-mode plots, correlating to the expected range of *r*—the tensor-to-scalar ratio which defines the energy scale of the inflationary event—from 0.001 to 0.05. Exact value of *r* can only be found from the amplitude of the B-mode curve which is still under investigation [47]. Thus a range of possible *r* values is used for prediction, but only one B-mode power spectrum (blue) is expected to be measured.

7.1 Temperature Power Spectrum Explained

The greatest peak at 1° indicates the horizon scale [48]. These waves happened to have the photon-baryon fluid falling moving together and reaching greatest density at the point of recombination [48]. The trough right after the highest peak represents the waves where the photon-baryon fluid happened to have just moved and averaged out, reaching mean density [48]. The second peak is where some waves reach the rarefaction point (region of least matter

density) [48]. This process continues to produce multiple peaks and troughs with decreasing amplitudes as angular scale decreases.

Since the recombination epoch was not instantaneous, waves with higher frequencies are able to fluctuate in density during this epoch, creating the damping tail of the power spectrum [48]. This is known as silk damping.

8. Project Methods

8.1 Introduction to Data Analysis Techniques

In the Project Methods , I use a NASA CAMB (Code for Anisotropies in the Microwave Background) simulation and CMB analysis github tools[1] to plot the temperature CMB power spectrum using Python. Note that all figures in this section and beyond are plots I generated using Python, unless specified otherwise.

The temperature power spectrum is the expected behaviour of the CMB, and CMB experiments like WMAP, Planck, and ACT (Atacama Cosmology Telescope) have confirmed this behaviour to high precision (e.g. [1, 3, 4]). However, I use the NASA CAMB simulation of the CMB temperature power spectrum as a clean laboratory for understanding the behaviour of CMB maps without experimental and galactic noise. In addition, I use the temperature simulation to understand experimental, galactic, and atmospheric noise as well as experiments' filtering techniques—which will be discussed below—by learning how to simulate such noise onto the clean signal.

The first analysis step I take for the NASA CAMB theoretical CMB temperature signal is a flat sky approximation. A flat sky approximation requires taking a small patch around 10° by 10° of sky of CMB measured with mathematical equations altered slightly, and is also used in obtaining the power spectrum.

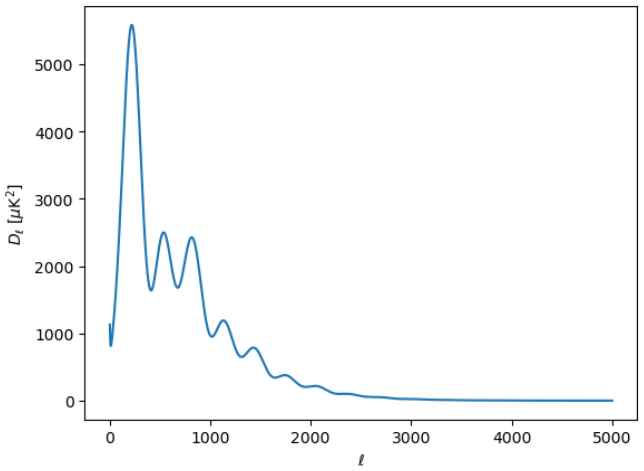

[Figure 6. Angular power spectrum generated in the clean laboratory; the horizontal axis denotes the angular frequency ell, the vertical axis denotes the extent of temperature variations]

The steps include: generate a 2D power-spectrum; generate a Gaussian random map; multiply the two together; and use fourier transform to result into a real space map.

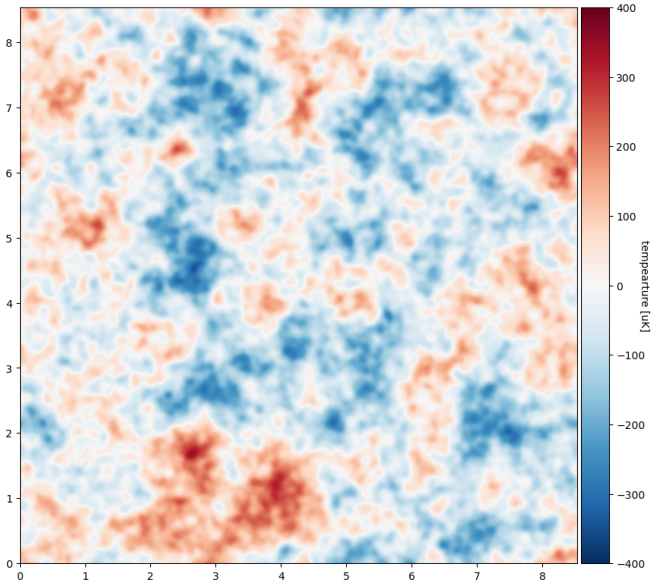

[Figure 7. Real space map of simulated CMB]

8.2 Adding Foregounds to the Simulated CMB

Foreground noise is noise from the galaxy and the universe that hinders direct data collection of the CMB [49]. There are mainly 2 types of foreground noises classified according to the characteristics of their sources, as is illustrated below.

In this section, I make a point source map in order to simulate how foreground noises affect the results of measurements of the CMB. Point sources are bright objects in the sky, such as Active Galactic Nuclei (AGN), Dust Star

1 https://github.com/jeffmcm1977/CMBAnalysis_SummerSchool/tree/master

Forming Galaxies (DSFGs), and any stars or bright galaxies that appear like a bright spot [49]. There are two main distributions discussed here for the sources. There are the poisson distribution sources, referring to a rather faint distribution of sources with a poisson distribution of brightness that originate from older galaxies. The other are the exponential sources, which are a small number of very bright sources with exponentially falling source count, usually from a nearby planet or a bright star or younger galaxy.

In order to simulate a raw sky, the point sources are simulated in the above two ways. The histogram data of the two different point sources shows the poisson map having a centred peak, while the exponential map having multiple peaks and troughs, as is provided below.

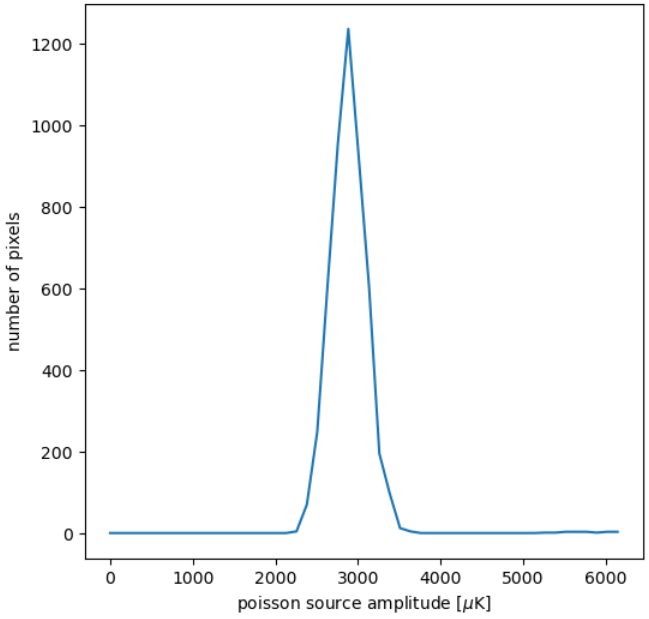

[Figure 8. Histogram for poisson sources]

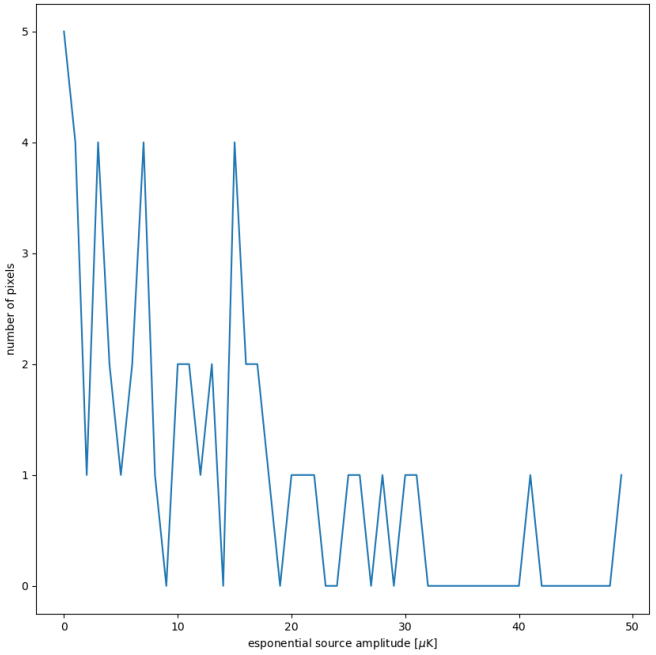

[Figure 9. Histogram for exponential sources]

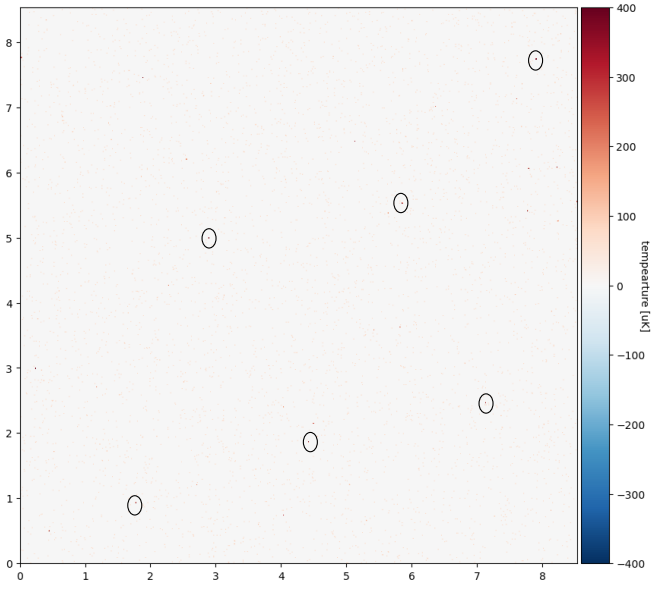

[Figure 10. Raw sky with some faint point sources circled]

SZ (Sunyaev-Zeldovich) maps are also made. SZ addresses the phenomena of the boost of energy that a CMB photon gets when it interacts with a relativistic electron travelling close to the speed of light [34]. Relativistic electrons come from galaxy clusters. Therefore, the SZ effect is useful in using the CMB photons to understand the behaviour of galaxy clusters and the evolution of galaxy formation [34]. With the simplified assumption of identical angular sizes between the clusters, SZ maps are thus simulated.

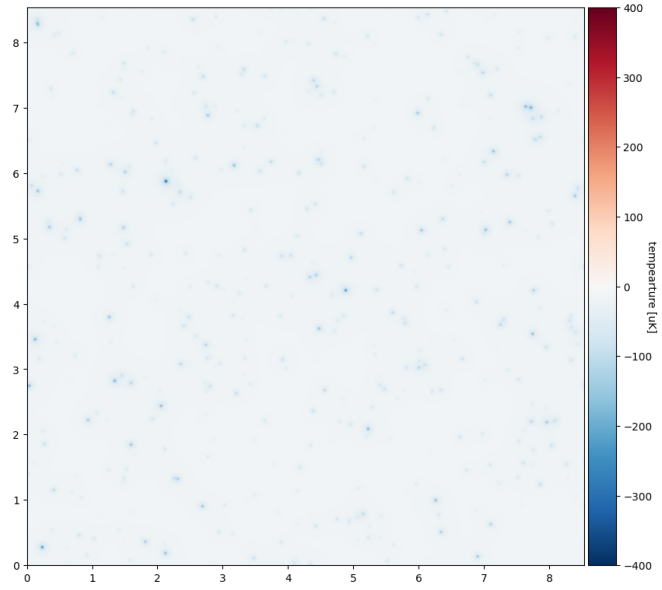

[Figure 11. SZ maps]

Combining the CMB anisotropy, a point source map, and an SZ map, a full sky map is hence produced.

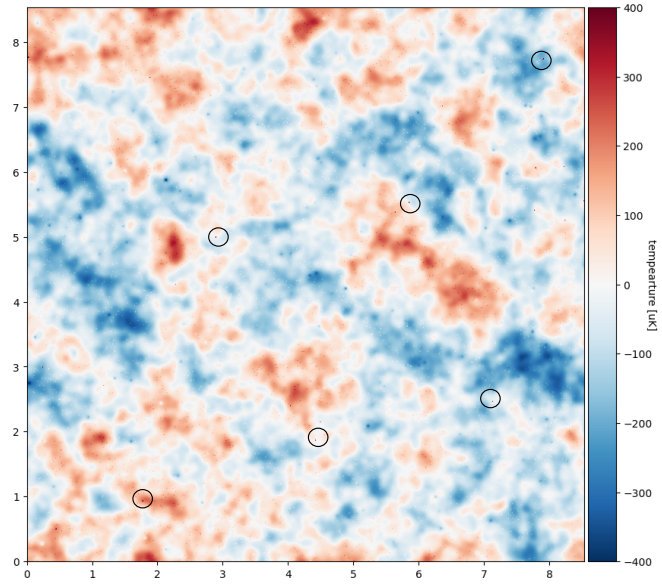

[Figure 12. Full sky map with all noises infused and some faint sources circled]

8.3 Instrument Beam, Instrument Noise, and Filtering

In this section, I explore the three main instrument noises that interfere with obtaining a clear CMB image. The white noise is common in signal processing where there's random Gaussian noise with equal intensity at different frequencies of CMB measurements; atmospheric noise is from the water vapour in the atmosphere and turbulence in the clouds; 1/f noise is low frequency noise where its power is inversely proportional to its frequency, this behaviour is typical of CMB (superconducting) detectors.

Plots specifying each noise show the following results.

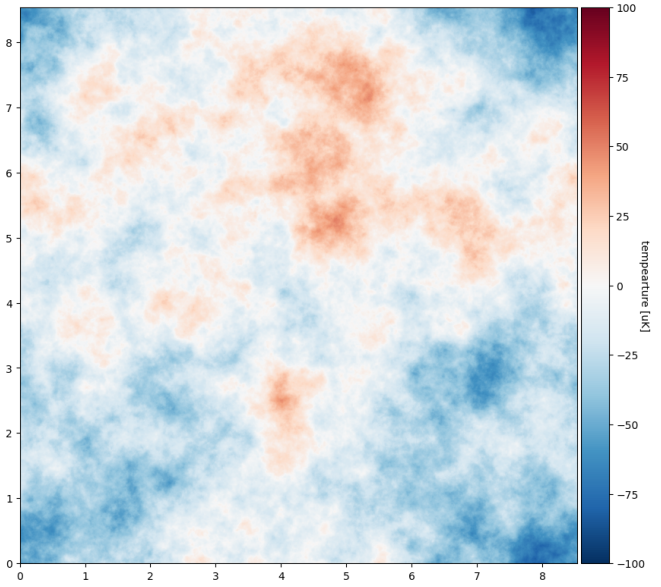

[Figure 13. Atmospheric noise at level 0.1]

The atmospheric noise distribution at level 0.1 in Figure 13, with white noise and 1/f noise at 0, makes the CMB blurrier, but retaining most of its patterns and characteristics.

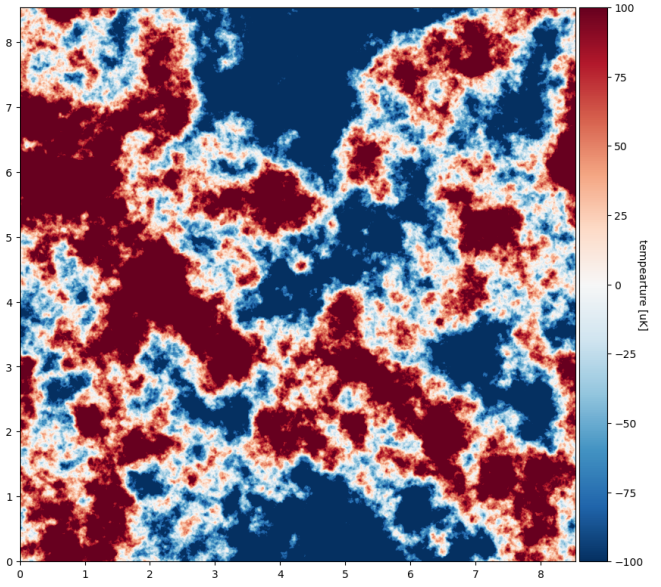

[Figure 14. Atmospheric noise at level 0.8]

As atmospheric noise increases in level as shown in Figure 14, CMB data collection becomes significantly hindered, only showing general patterns with a lack of precision.

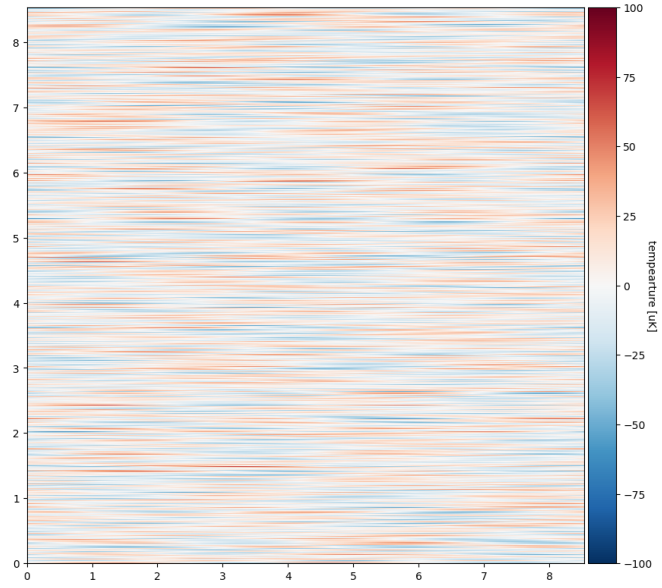

[Figure 15. 1/f noise at level 0.2]

The 1/f noise distribution at 0.2 in Figure 15, with white and atmospheric noise at 0, makes the CMB very streaky. The horizontal streaks cut out most of the CMB patterns. Calibration of detectors are needed when 1/f noise becomes overly prominent.

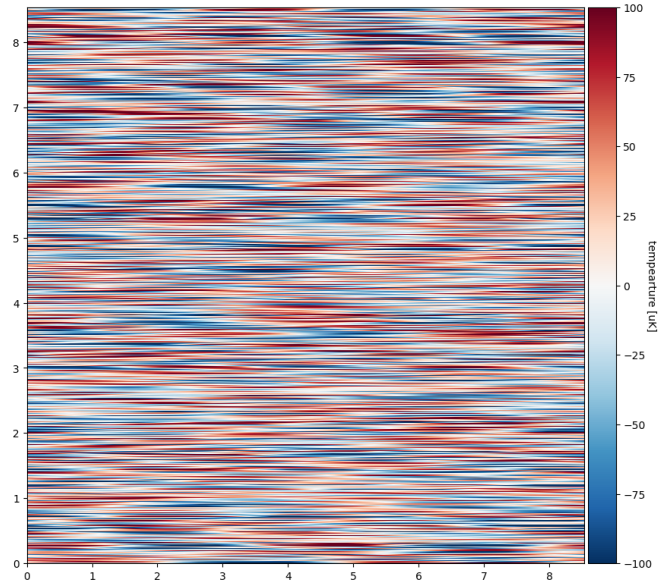

[Figure 16. 1/f noise at level 0.7]

Measurements of CMB are significantly hindered in Figure 16 at this 1/f noise level.

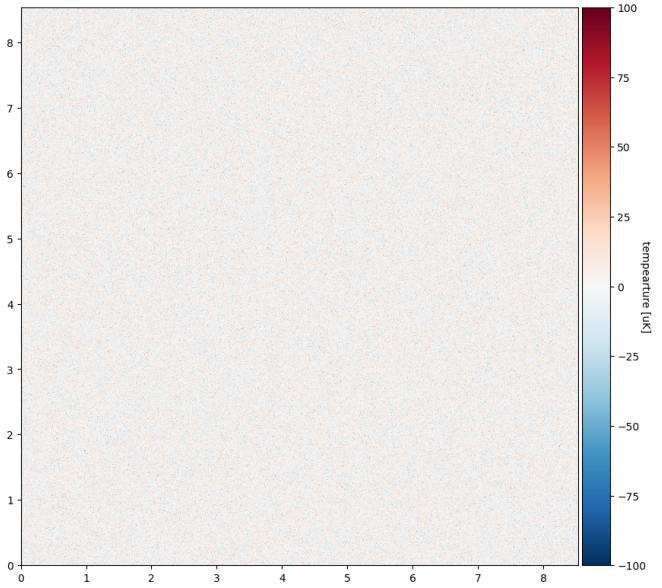

[Figure 17. White noise at level 10]

The white noise distribution at level 10 in Figure 17, with atmospheric noise and 1/f noise at 0, blocks most of the CMB patterns. The graph appears very grainy, with such graininess increasing as the level of white noise increases. Through masking out certain fourier modes, the above noises can be roughly filtered from the CMB.

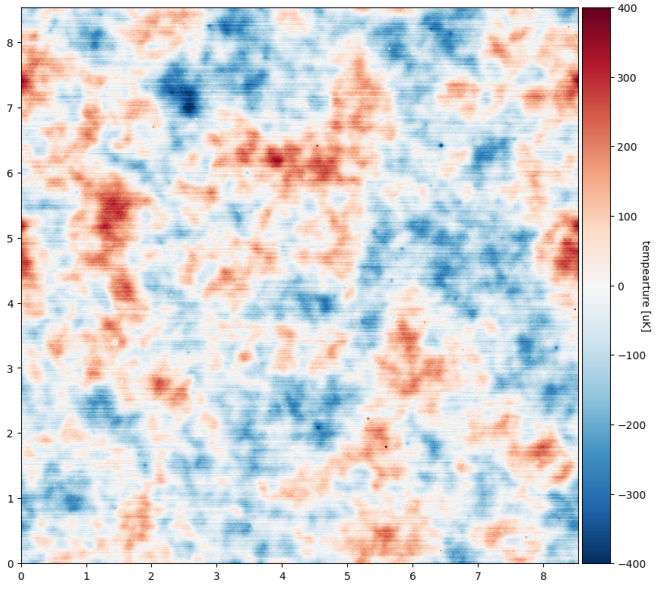

[Figure 18. CMB map simulated with noise]

The above map shows what a more realistic measurement of CMB data would appear, with point sources and SZ noises combined.

8.4 Map Analysis (Apodization)

In the CMB map, because we take measurements by square chunks of data (i.e. the 10 degree by 10 degree mentioned in section 1), part of the CMB signal gets cut off,

which adds an interfering factor known as an edge effect [50]. Edge effect occurs because the fourier transform does not work with straight edges of square arrays as it treats them as periodic boundaries [51]. Thus, the CMB maps need to be apodized – modification of the signal, which is smoothing out the edges in this particular case – before being transformed into power spectrums. By selecting different windows, the apodized map also varies in appearance.

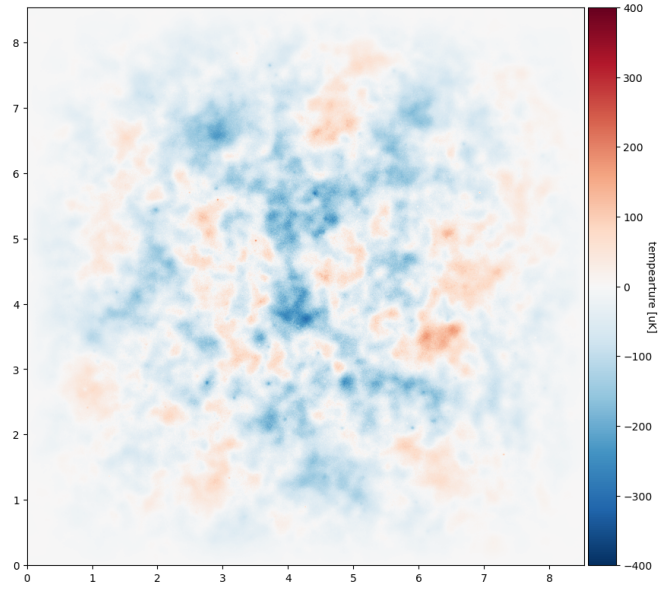

[Figure 19. Apodization done using a cos() x cos() window]

Figure 19 shows a cos() x cos() apodized map. This window function has its centre clear and fainting towards the edges, which allows us to analyse the middle region of the data without being affected by the edge effect. More methods of apodization are illustrated below, though they will not be used in further experiments because they do not eliminate edge effects as successfully as the cos() x cos() window.

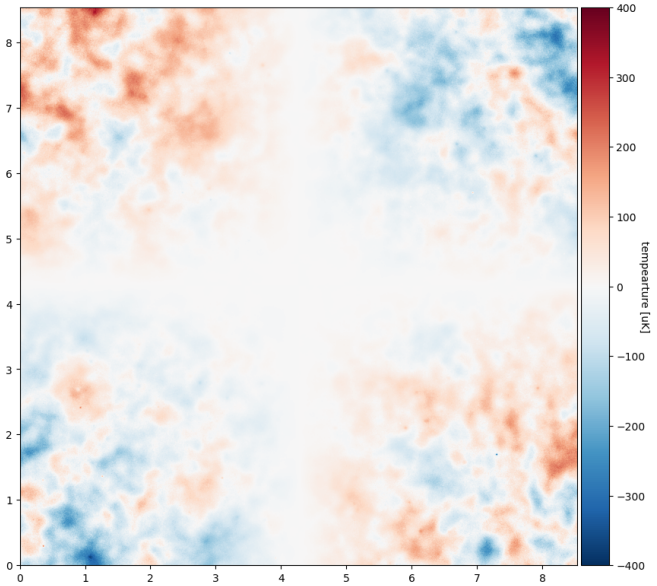

[Figure 20. Apodization done using a sin() x sin() window]

The sin() x sin() apodized map has its edges clear and fainting towards the centre.

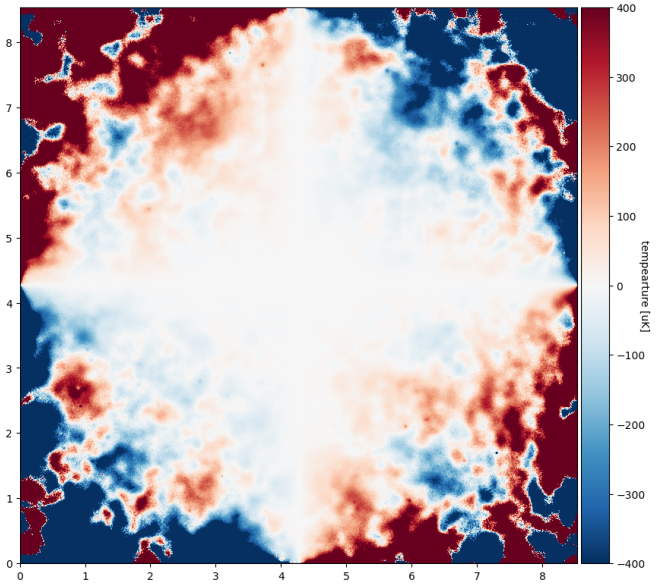

[Figure 21. Apodization done using a tan() x tan() window]

The tan() x tan() apodized map has its centre nearly absent with strongly-emphasised edges.

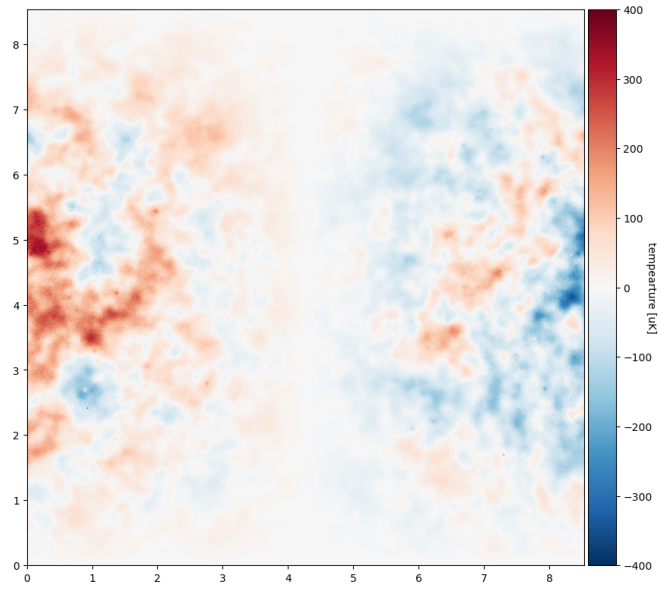

[Figure 22. Apodization done using a sin() x cos() window]

The sin() x cos() apodized map has its horizontal edges and its centre fainting, while the fainting edges change to the vertical ones when switched to the cos() x sin() apodized map.

8.5 Map Analysis

Data analysis using real CMB data is shown in this section.

The following CMB data is collected by the Atacama Cosmology Telescope (ACT), a CMB telescope that focuses on how the universe began and evolved as well as its components [52]. The ACT experiment has two main goals. One is to further the measurements of parameters that describe the primordial universe [52], which allows us to have a clearer idea of how the universe evolved over time. The other is to measure distant, large clusters of galaxies and respective environments, so as to narrow down the possibilities of different models of how the universe behaved in its infancy [52], enabling us to understand the evolution of cosmic structures, as well as the history of old galaxies. In order to achieve its goals, ACT is equipped with 3000-5000 detectors (e.g. [3]).

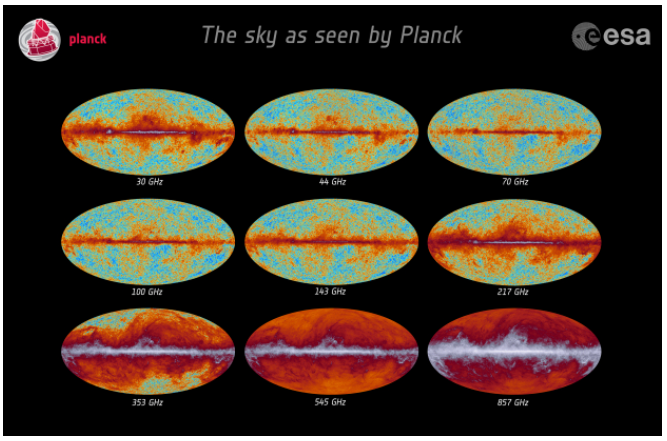

[Figure 23. Measurements of CMB by the Planck telescope. Image from [53]]

Data of different gigahertz and thus different frequency bands are being used here. This is done so as to synchronise background measurements and hence better subtract noise and pick up CMB data. CMB is usually most evident in the frequency bands between 70 to 210 GHz. However, a lot of the noise discussed in this section – including galactic and atmospheric noise when using ground-based telescopes, or mainly galactic noise when using a satellite telescope – are at frequencies above 210 GHz [54]. But since this paper focuses on ground-based experiments, its data will not go above 220 GHz.

At 220 GHz, atmospheric noise plays a rather significant role [54], which is evident from Figure 24, especially when comparing with the 148 GHz data in Figure 25.

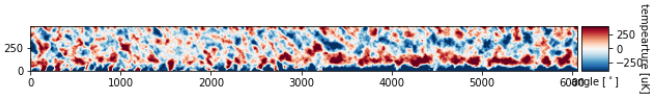

[Figure 24. ACT CMB data generated at 220 GHz]

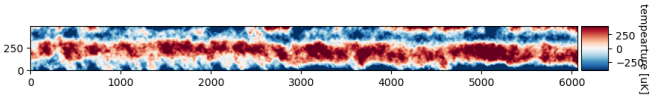

[Figure 25. ACT CMB data generated at 148 GHz]

The analysis in previous sections is done using square patches, thus square patches are taken out of the long strip of ACT data to be used to compute the power spectrum using the methods mentioned above.

Firstly, I apodize using a cosine function for the 148 GHz ACT data.

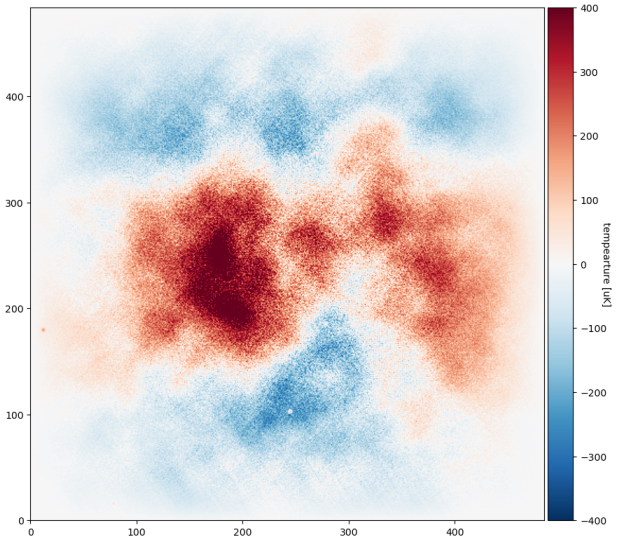

[Figure 26. 148 GHz ACT data after apodization]

Then, I simulate a theoretical CMB map with noise in order to compare the theorised power spectrum with similar noise with the actual ACT data above.

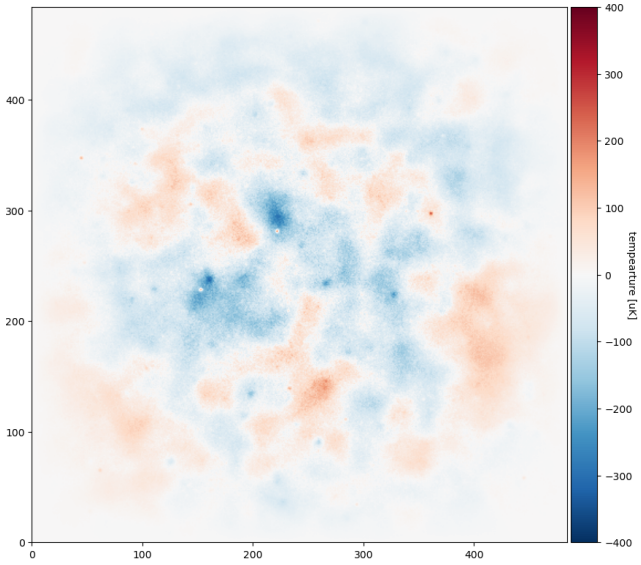

[Figure 27. Expected CMB data with apodization]

Finally, I compute it into a power spectrum.

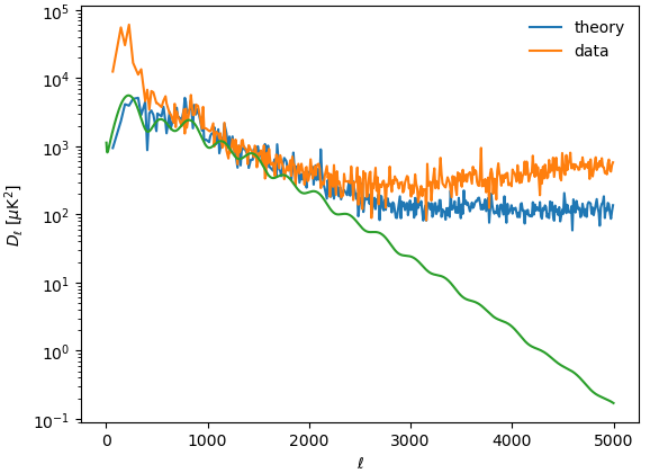

[Figure 28. Power spectra based on theory (blue) and data (orange)]

The green plot in Figure 28 shows the expected CMB power spectrum under the assumption of zero noise. This prediction at high *l* values has not yet been confirmed by measurements due to foreground, atmospheric, and instrumental noise.

As is displayed in Figure 28, the instrumental noise in ACT data in orange has a higher amplitude at very low *l*'s and at *l* greater than 2500 than the theorised one (where artificial noise has been added to simulate similar noise level, including atmospheric noise as well as SZ and Point sources) in blue. This results in greater differences between the two power spectra at high ell scales. The particular patch of sky being measured is also an influencing factor.

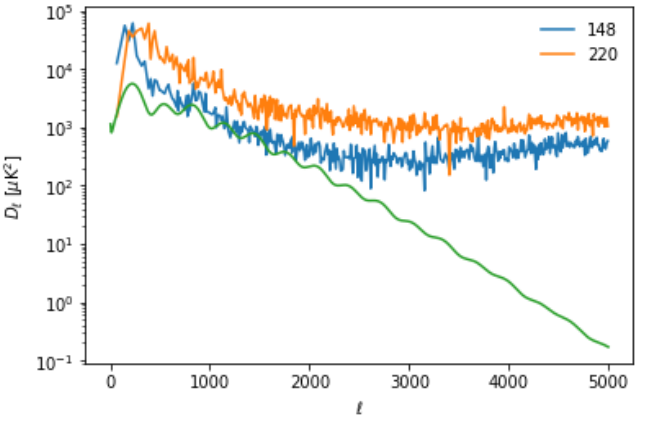

[Figure 29. Power spectra based on 148 GHz (blue) and 220 GHz data (orange)]

As is shown in Figure 29, power spectra from different frequency bands have generally the same shape but have different magnitudes of data due to the presence of noise. Comparing data of different frequency bands, the disparity between the two is due to the presence of more atmospheric noise in the 220 GHz data [54]. The two power

spectra generally have similar features, which confirms the accuracy of ACT measurements.

8.6 Map Analysis

In this section, I will focus on how to translate theoretical CMB data into power spectra.

The power spectra that we will explore include the TT, EE and TE power spectra. TT and EE power spectra are auto-correlations [46]. TT is the temperature power spectrum, and EE is the E-mode power spectrum. These two power spectra are related in the sense that they both explain cosmic structural formation [46].

Recall the process of baryonic acoustic oscillations, where gravity acted to bring the baryons together causing them to heat up, then the increase in pressure pulls them apart [22]. These two forces can be viewed as the tendency to create overdense anisotropies versus the tendency to erase them [22], which tells us that overdense regions generally have higher levels of E-mode polarisation. Meanwhile, according to the integrated Sachs-Wolfe effect [36], places with overdensities generally have cooler temperatures. Thus, whenever there is a peak in TT, a corresponding trough occurs in EE. The TE power spectrum measures the correlation between the T and E data.

Below are figures of TT, EE, BB and TE power spectra.

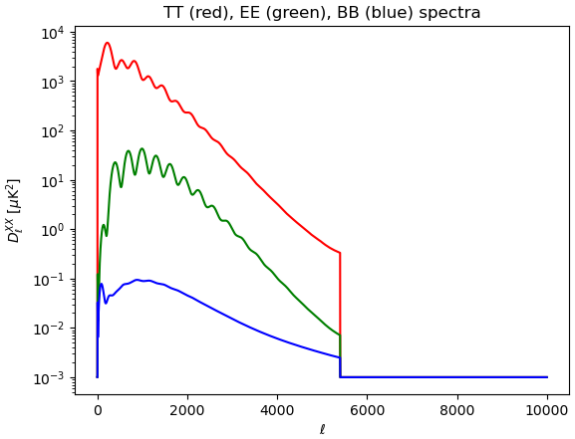

[Figure 30. TT, EE, and BB power spectra]

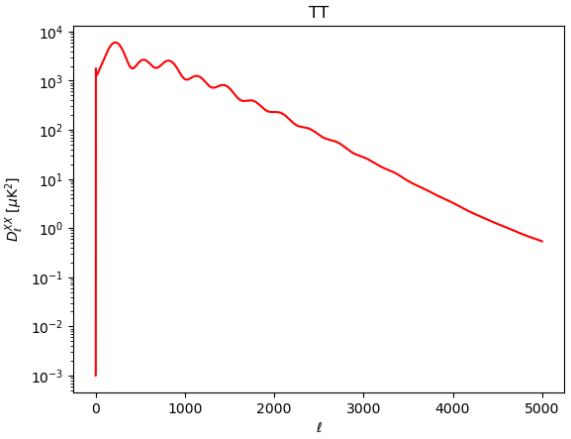

[Figure 31. TT power spectrum zoomed in for l = 0-5000]

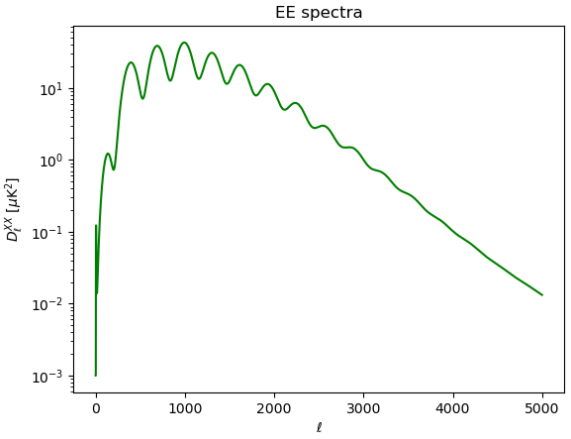

[Figure 32. EE power spectrum zoomed in for l = 0-5000]

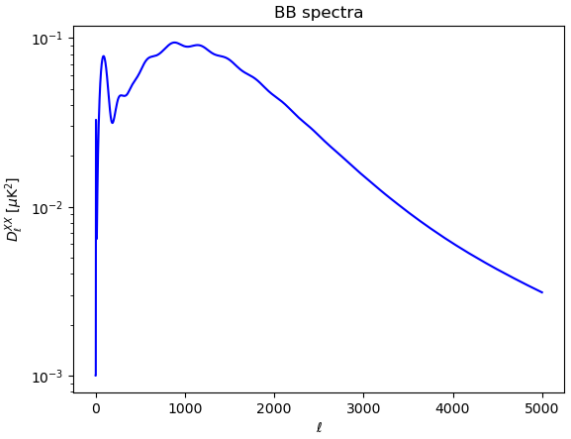

[Figure 33. BB power spectrum zoomed in for l = 0-5000]

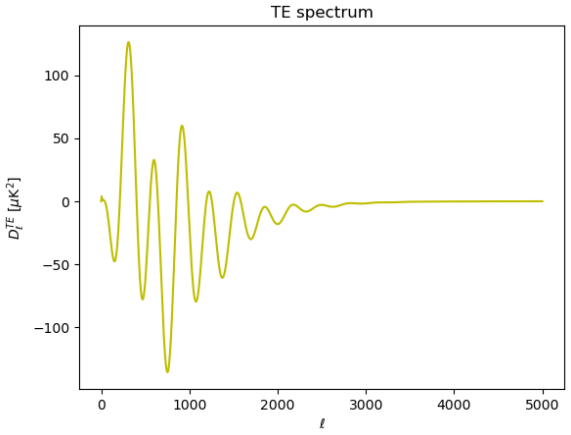

[Figure 34. TE power spectrum zoomed in for l = 0-5000]

Next, we will look at how the measurements of Stokes parameters Q and U allow us to indirectly obtain information on E and B-modes.

The Stokes parameters are measurements of the extent of polarisation of electromagnetic waves – in this case, the CMB. There are in total 4 Stokes parameters, of which we will look at the two that apply to CMB polarisation the most. The parameter Q measures the degree of polarisation along the vertical and the horizontal components, while the parameter U measures that of two diagonal directions [55].

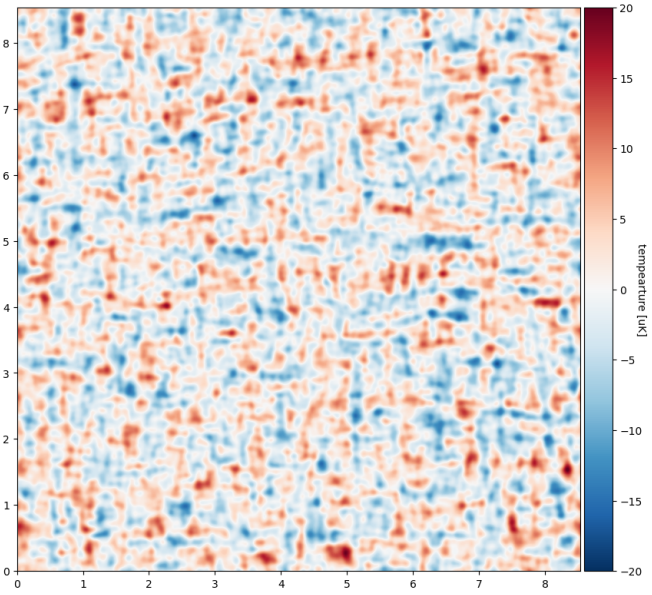

[Figure 35. Measurements of the parameter Q]

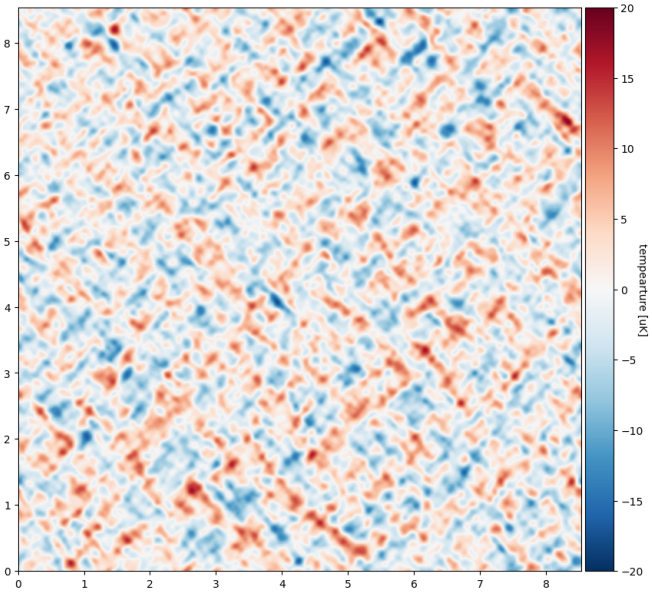

[Figure 36. Measurement of the parameter U]

Actual E and B-mode polarisation are linked with parameters Q and U by the following equations.

$E = Q\cos(2\psi) + U\sin(2\psi)$

$B = -Q\sin(2\psi) + U\cos(2\psi)$ [55]

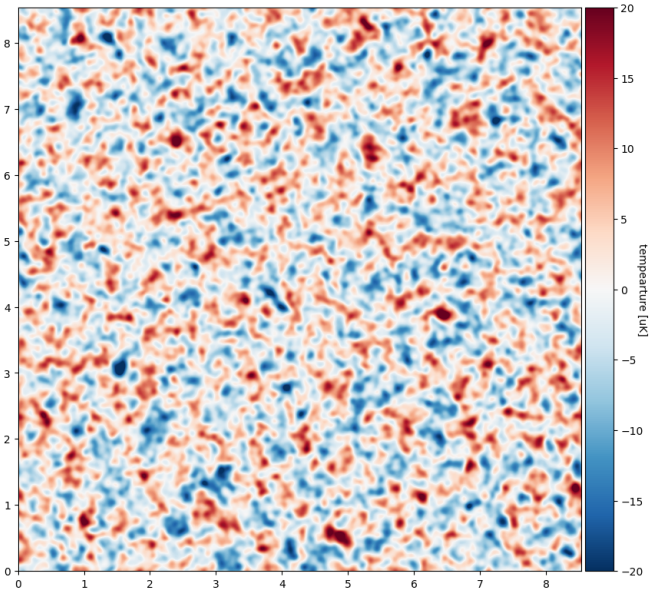

[Figure 37. Calculated result of E-mode polarisation]

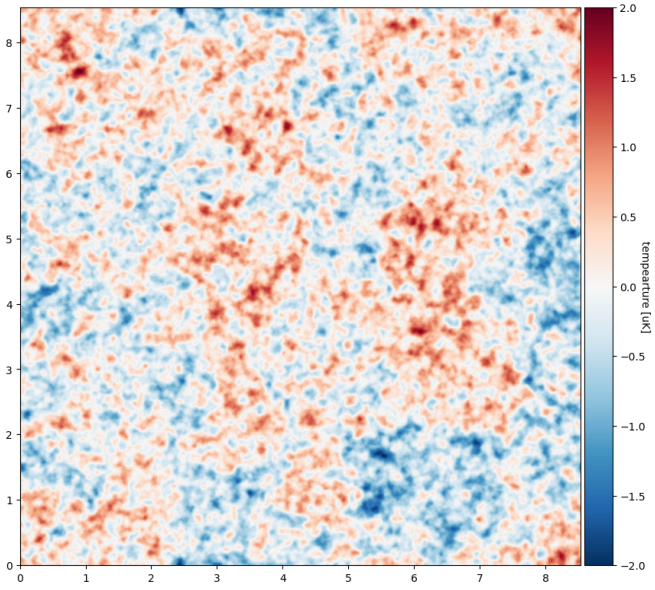

[Figure 38. Calculated result of B-mode polarisation]

Recall that B-mode polarisation that relates directly to inflation have not been detected, thus the B-mode simulations in this section have not yet been corroborated with real data like that of the E-mode.

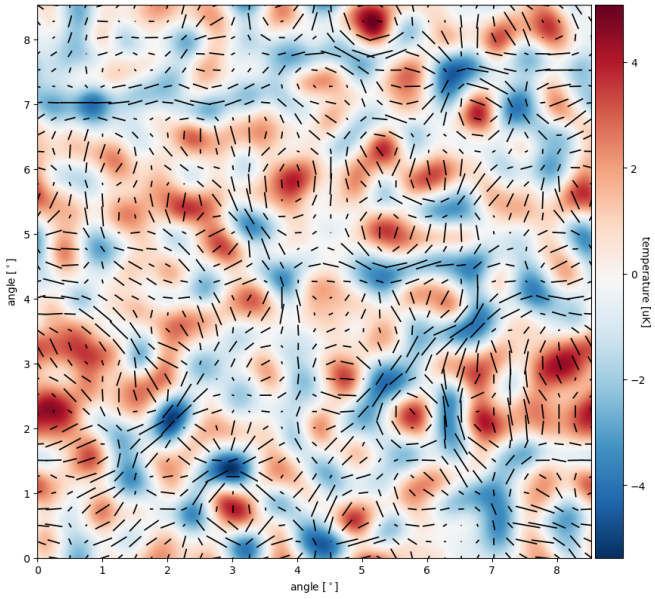

[Figure 39. CMB data with polarisation pattern overlapped]

In the above diagram, the length of the lines indicates the magnitude of the E-mode polarisation, while the different colours indicate the temperature. Blue regions which are colder generally have more diagonal lines, which means more polarisation is occurring at these cold regions.

9. Exploring Different Versions of the Universe through the CMB

Recall that for a regular universe, the temperature of CMB is at around 2.73 Kelvin, and the curvature parameter in the Big Bang model is 0 due to its near perfect flatness.

In this section, I will first generate the power spectra for the regular universe. Then I will consider three cases of hypothetical universes, respectively having temperature of CMB at 8 Kelvin , temperature of CMB at 5 Kelvin, and curvature parameter at 1 with temperature unchanged, and compare their features with that of our current one.

9.1 Current Universe (expected behaviour)

Before any discussions on hypothetical universes, I will first explore our regular universe and its expected behaviours in terms of its power spectra. Some of the following behaviours are mentioned above in previous sections, but will be gone through again for the sake of better comparison.

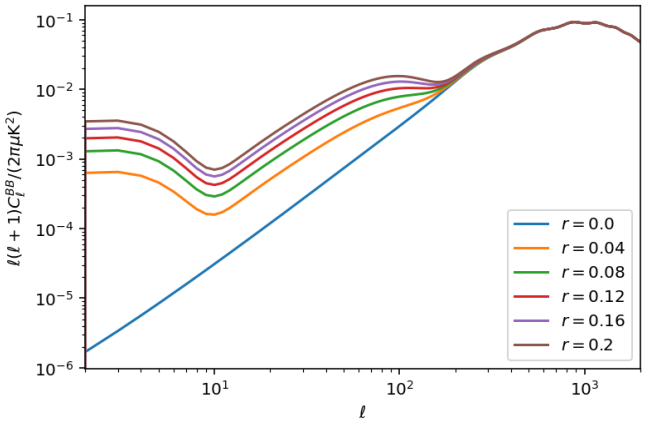

[Figure 40. B-mode polarisation of the regular CMB]

Above is the expected data of B-mode polarisation with r = 0.0 to r= 0.2.

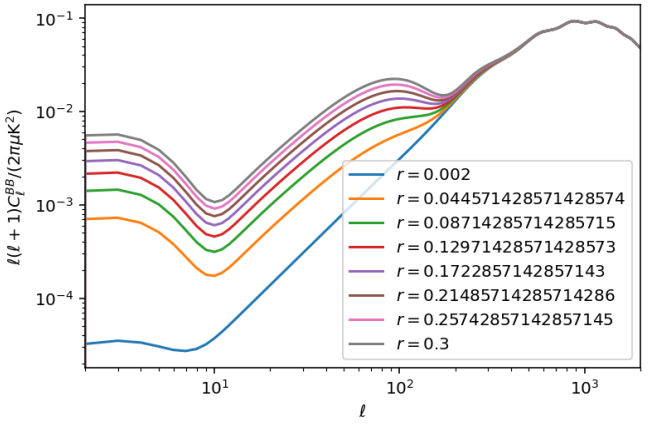

[Figure 41. B-mode polarisation of the regular CMB]

Figure 41 is the expected data of B-mode polarisation with r = 0.002 to r= 0.3. The uniform dip at around 10 ell indicates the presence of inflation. All r values converge at around 200 ell.

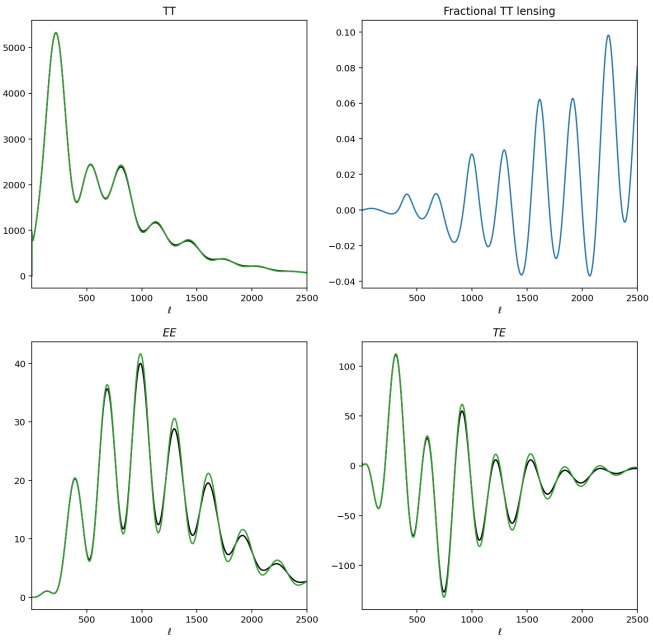

[Figure 42. TT, EE, and TE power spectra of the regular CMB]

The TT power spectrum of the regular universe shows a significant peak at around 1-200 ell, with other minor peaks occurring with decreasing magnitudes as l value increases.

The EE power spectrum has its highest peak at around 1000 ell, with peaks of decreasing amplitudes on both sides.

The TE power spectrum has significant fluctuations contributing to high peaks and low troughs between the range of 250 ell to around 1000 ell, while magnitudes of such fluctuations gradually cease as ell increases.

9.2 Universe at TCMB = 8 K

In this section, I explore similar features of the universe when the temperature of the CMB is at 8 Kelvin. Since the temperature of the CMB has cooled down over time, a universe with higher CMB temperature can be seen as one that is further back in time.

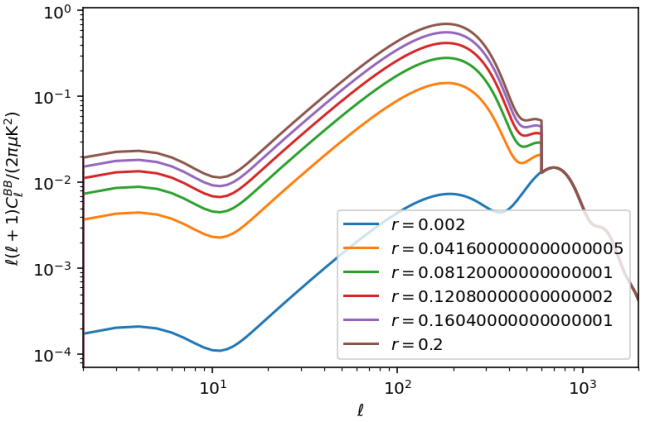

[Figure 43. B-mode polarisation of the CMB when TCMB = 8 K]

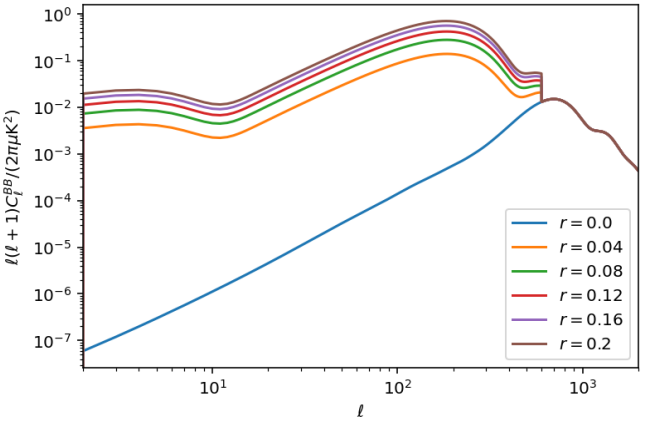

[Figure 44. B-mode polarisation of the CMB when TCMB = 8 K]

The above two graphs are data of B-mode polarisation of the CMB when its temperature is at 8 Kelvin, with different r value ranges assigned.

Compared to that of a regular universe, the vertical-axial value of this hypothetical universe in Figures 43 and 44 increases by approximately 10 times. There continued to be a dip at around 10 ell, but with less significance. A precipitous change in value occurs at around 800 ell, which is absent in Figure 40 and 41.

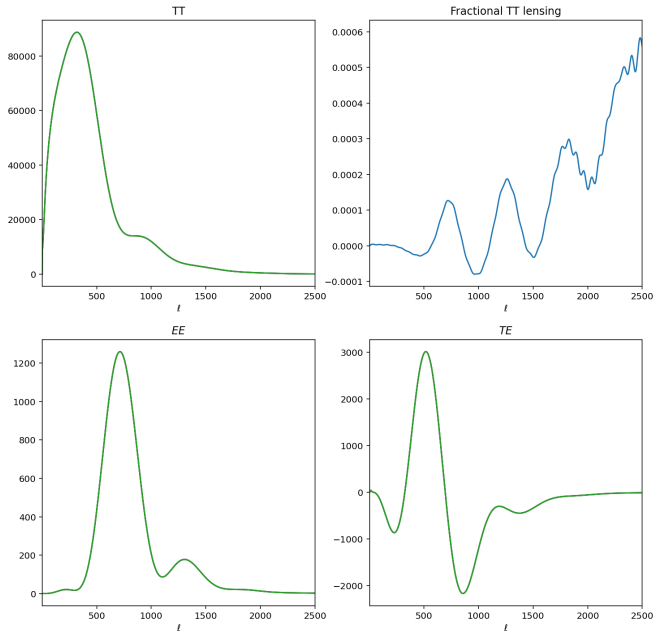

[Figure 45. TT, EE, and TE power spectra of the CMB when TCMB = 8 K]

Figure 45 shows the power spectra for the hypothetical universe. Common to all the spectra are significant increases in the vertical-axial values, as well as their much more shapeless appearances. The higher vertical-axial values are indications of the more powerful signals, which results from the higher temperature, while the shapeless appearances are due to the less solidified behaviours of matter.

The TT power spectrum continues to demonstrate a major peak at around 100-200 ell.

The EE power spectrum has its major peak at around 750 ell, while the regular universe has the same peak at around 1000 ell.

The TE power spectrum has its major peak at around 500 ell, and a significant dip at around 900 ell, which generally follows that of the regular universe, with the figure shifted to the right to about 200 ell.

Though all the above power spectra for the regular universe had other significant peaks and troughs, they are no longer observable under TCMB = 8 K.

9.3 Universe at TCMB = 5 K

In this section, I explore the universe at a CMB temperature of 5 Kelvin.

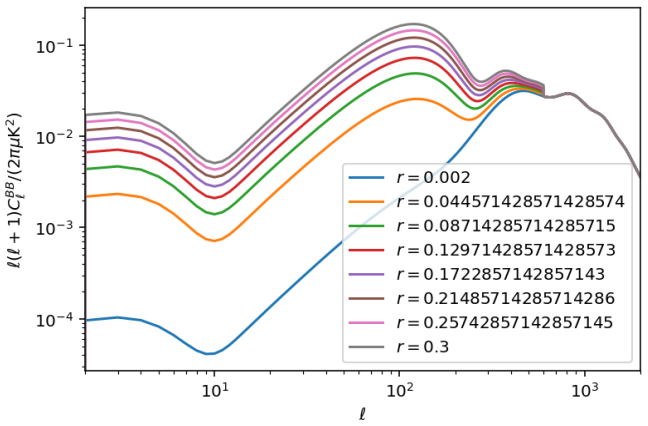

[Figure 46. B-mode polarisation of the CMB when TCMB = 5 K]

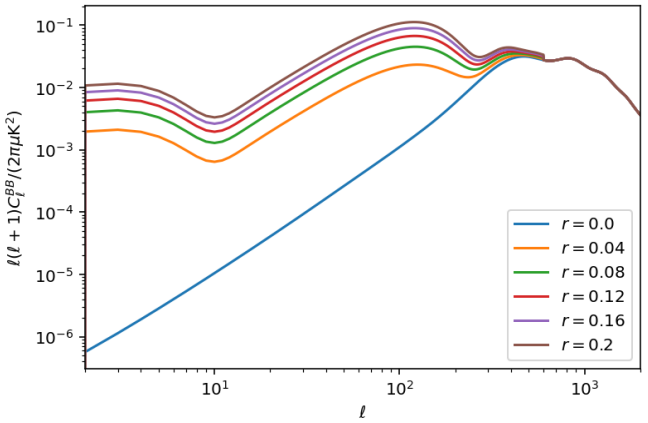

[Figure 47. B-mode polarisation of the CMB when TCMB = 5 K]

Here the values on the vertical axis are slightly higher, but generally remain similar to that of the regular universe. This is because – considering the process of CMB cooling down, the universe with TCMB of 5 Kelvin is closer to today's universe than that of the 8 Kelvin discussed above. The ell value that corresponds to the dip is around 10 in both cases. The only major difference is when the range of r value graphs converge, which is around 800 ell in this case but around 200 ell in the regular universe.

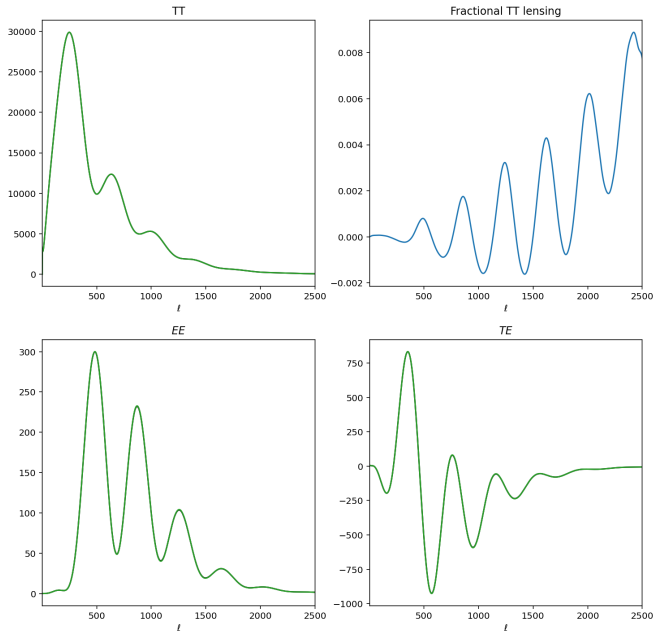

[Figure 48. TT, EE, and TE power spectra of the CMB when TCMB = 5 K]

At TCMB = 5 K, the power spectra demonstrate significantly more traits that the regular universe has. Aside from the characteristic peaks and troughs, the power spectra in this case is much less shapeless compared to that of when TCMB = 8 K, but still lacks fluctuations compared to that of the normal universe because certain information of the parameters have not yet solidified and well-defined in this younger universe. The value along the vertical axis also increases in this case, but not as prominent as the previous case.

In general, it seems that higher temperatures being further back in time provides slightly more information on B-mode power spectra, with the dip more defined and the point of convergence of different r values more significant. Meanwhile, there is a loss of information in the other power spectra due to the reasons stated above.

9.4 Universe at Curvature Parameter = 1

In this section, I will explore a universe with curvature parameter = 1. This means that this universe will no longer be perfectly flat, and that it will demonstrate negative curvature.

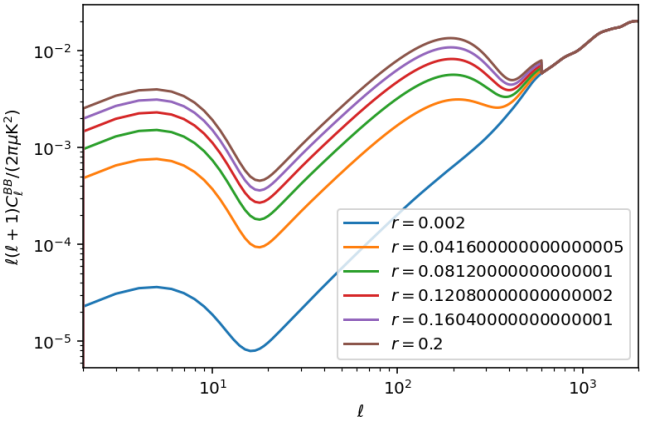

[Figure 49. B-mode polarisation of the CMB when Curvature Parameter = 1]

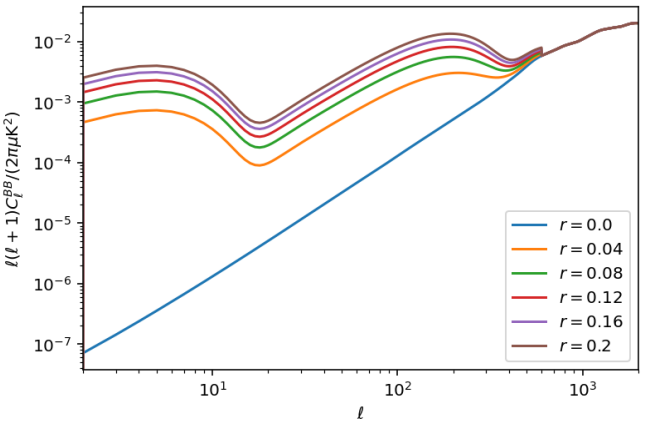

[Figure 50. B-mode polarisation of the CMB when Curvature Parameter = 1]

In this case, the significant dip occurs slightly rightwards of 10 ell, with all the r values converging at around 700 ell. Both features shifted rightwards compared to that of the regular universe.

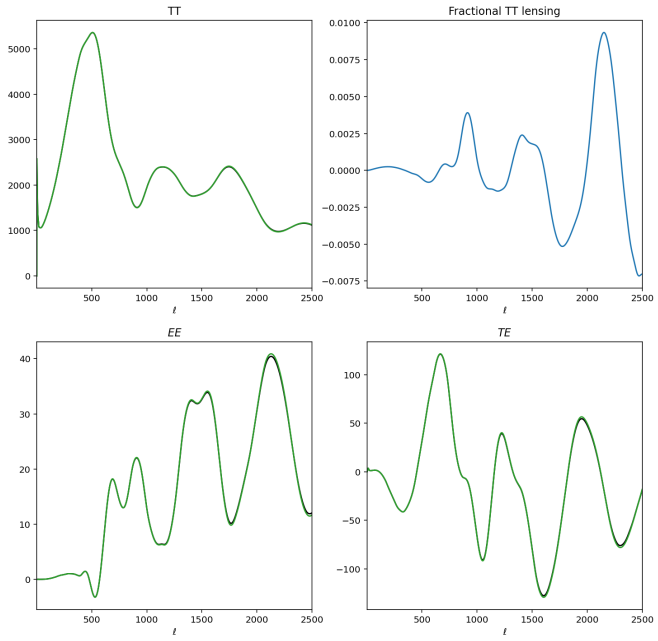

[Figure 51. TT, EE, and TE power spectra of the CMB when Omega k = 1]

There are significant differences in shapes between the power spectra of the negatively curved universe and the regular flat universe.

The TT power spectrum here demonstrates its major peak at 500 ell, which is around 300 ell rightwards than the regular universe. The figure appeared to be stretched, with the two following minor peaks corresponding to that of the regular universe but far rightwards than their original ell values.

The EE power spectrum here has its major peak at around 2200 ell with decreasing amplitudes as ell decreases, while the one in the regular universe has the major peak at around 1000 ell and amplitudes decreasing on both sides. I suspect that this figure is also stretched such that only the leftward region of the original EE spectrum is demonstrated here. This might have indicated loss in information on structure formation as fewer peaks are shown.

The TE power spectrum also appears similarly stretched, with its major peak occurring at around 600 ell, nearly 400 ell rightwards of its original position.

10. Conclusion

To conclude, this research paper explores how the Cosmic Microwave Background has evolved over time as well as its various features. It also delves into how actual data collection occurs, and how behaviours of the universe can be altered differently through changing certain key parameters. The CMB analysis code on github has made it possible for me to reproduce the codes and plots for that work as well as expand on the codes to explore different versions of the universe for my own project. Through this research, I have gained a better understanding of how the universe functions as well as the significance of some of its behaviours.

Acknowledgements

Assistance received for this project include the github code for CMB analysis (link: https://github.com/jeffmcm1977/CMBAnalysis_SummerSchool/tree/master) from which I could reproduce my own codes, as well as references indicated in the last section.

References

[1] Planck Collaboration, Planck 2018 results. VI. *Cosmological parameters* (2021), arXiv:1807.06209v4
[2] Henning, J.W., et al., *Measurements of the Temperature and E-Mode Polarization of the CMB from 500 Square Degrees of SPTpol Data* (2018), arXiv:1707.09353
[3] ACTPol Collaboration, *The Atacama Cosmology Telescope: Two-Season ACTPol Spectra and Parameters* (2016), arXiv:1610.02360
[4] WMAP Collaboration, *Nine-Year Wilkinson Microwave Anisotropy Probe (WMAP) Observations: Cosmological Parameter Results* (2013), arXiv:1212.5226v3
[5] Simons Observatory Collaboration, *The Simons Observatory: Science goals and forecasts* (2019), arXiv:1808.07445v2
[6] "*The Big Bang Theory.*" Medium, 12 June 2021, https://guyfromthecosmos.medium.com/the-big-bang-theory-b2a984b1e10f.
[7] Liddle, A.R., et. al., *An Introduction to Cosmological Inflation*, (1999), arXiv: astro-ph/9901124
[8] Rajantie, A., *Magnetic Monopoles in Field Theory and Cosmology*, (2012). arXiv: 1204.3073
[9] "*WMAP inflation theory*." NASA, https://wmap.gsfc.nasa.gov/universe/bb_cosmo_infl.html. Accessed 12 August 2023.
[10] "*WMAP CMB fluctuations*." NASA, https://wmap.gsfc.nasa.gov/universe/bb_cosmo_fluct.html. Accessed 12 August 2023.
[11] "*Density Parameter.*" COSMOS, https://astronomy.swin.edu.au/cosmos/d/density+parameter. Accessed 12 August 2023.
[12] Jones, A., et. al., *The Inflation Theory: Solving the Universe's Problems of Flatness and Horizon*, (2016).
[13] White, M., et. al., *Anisotropies in the CMB*, (1999), arXiv: astro-ph/9903232
[14] Abbott, B., "*Microwave (WMAP) All-Sky Survey*", Hayden Planetarium, https://web.archive.org/web/20130213023246/http://www.haydenplanetarium.org/universe/duguide/exgg_wmap.php. Accessed 12 August 2023.
[15] Pettini, M., "*Recombination and the Cosmic Microwave Background.*"

https://people.ast.cam.ac.uk/~pettini/Intro%20Cosmology/Lecture09.pdf. Accessed 12 August 2023.
[16] "*CMB Surface Of Last Scatter*." NASA, https://map.gsfc.nasa.gov/media/990053/index.html. Accessed 12 August 2023.
[17] Planck, M., *The Theory of Heat Radiation*, (1914).
[18] "*Ultraviolet catastrophe - Rayleigh-Jeans catastrophe.*" Nuclear Power, 27 Feburary 2022, https://www.nuclear-power.com/nuclear-engineering/heat-transfer/radiation-heat-transfer/ultraviolet-catastrophe-rayleigh-jeans-catastrophe/.
[19] Samtleben, D., et. al., *The Cosmic Microwave Background for Pedestrians: A Review for Particle and Nuclear Physicists*, (2008), arXiv: 0803.0834v
[20] Crockett, C., "*What do redshifts tell astronomers?*", EarthSky, 24 January 2021, https://earthsky.org/astronomy-essentials/what-is-a-redshift/.
[21] "*An Interactive Guide To The Fourier Transform.*" BetterExplained, https://betterexplained.com/articles/an-interactive-guide-to-the-fourier-transform/#:~:text=The%20Fourier%20Transform%20takes%20a,every%20cycle%20that%20was%20found. Accessed 12 August 2023.
[22] Bassett, B. A., et. al., *Baryon Acoustic Oscillations*, (2009). arXiv: 0910.5224v1
[23] Harrison, D. M., "*A 'Brief' Introduction to the Fourier Transform.*" 14 April 2011, https://faraday.physics.utoronto.ca/PVB/Harrison/FourierTransform.pdf.
[24] Gamow, G., *The evolution of the universe*, (1948).
[25] Wilson, R. W., *The Cosmic Microwave Background Radiation* (Nobel Lecture), (1978).
[26] Dicke, R. H., *The Measurement of Thermal Radiation at Microwave Frequencies,* (1946).
[27] "*COBE | Science Mission Directorate*." NASA, 29 July 2015 (last update), https://science.nasa.gov/missions/cobe.
[28] "*Wilkinson Microwave Anisotropy Probe (WMAP)*." NASA, 22 December 2017 (last update), https://map.gsfc.nasa.gov/.
[29] "*Planck | The Schools' Observatory*." National Schools' Observatory, https://www.schoolsobservatory.org/learn/eng/tels/spacetel/planck. Accessed 12 August 20233.
[30] Kruesi, L. "*Decoding the cosmic microwave background.*" Astronomy Magazine, 27 July 2018, https://www.astronomy.com/science/decoding-the-cosmic-microwave-background/.
[31] Challinor, A., et. al., *CMB Anisotropy Science: a review*, (2012), arXiv: 1210.6008v1
[32] Aghanim, N., et. al., *Secondary Anisotropies of the CMB*, (2007), arXiv: 0711.0518
[33] Silk, J., *Cosmic Black-Body Radiation and Galaxy Formation*, (1968).
[34] Birkinshaw, M., *The Sunyaev–Zel'dovich effect*, (1999).
[35] Sachs, R. K., et. al., *Perturbations of a Cosmological Model and Angular Variations of the Microwave Background*, (1967).
[36] Rees, M. J., et. al., *Large-scale Density Inhomogeneities in the Universe*, (1968).
[37] Komatsu, E., *Matter Adds Twist to Cosmic Microwave Background*, (2013).
[38] Campanelli, L., et. al., *Cosmic Microwave Background Quadrupole and Ellipsoidal Universe*, (2007), arXiv: 0706.3802
[39] Cabella, P., et. al., *Theory of Cosmic Microwave Background Polarization*, (2005), arXiv: astro-ph/0403392
[40] Chisari, E., "*Lensing B-modes in the Cosmic Microwave Background polarization*." Astrobites, 24 July 2013, https://astrobites.org/2013/07/24/lensing-b-modes-in-the-cosmic-microwave-background-polarization/.
[41] "*Gravitational waves*." LIGO Lab | Caltech, https://www.ligo.caltech.edu/page/gravitational-waves. Accessed 12 August 2023.
[42] Hu, W., et. al., *Mass Reconstruction with CMB Polarization*, (2001), arXiv: astro-ph/0111606
[43] Zaldarriaga, M., et. al., *Gravitational lensing effect on cosmic microwave background polarization*, (1998), arXiv: astro-ph/9803150
[44] Puye, "*Introduction to spherical harmonics.*" Puye's Blog, 5 February 2023, https://puye.blog/posts/SH-Introduction-EN/.
[45] Abazajian, K. N., et. al., *CMB-S4 Science Book*, (2016), arXiv: 1610.02743
[46] Hu, W., et. al., *Small Scale Cosmological Perturbations: An Analytic Approach*, (1995), arXiv: astro-ph/9510117
[47] Adachi, S., et al., *A Measurement of the Degree Scale CMB B-mode Angular Power Spectrum with Polarbear*, (2019), arXiv:1910.02608v1
[48] Freiberger, M., "*Cosmic peaks*." Plus Maths, 27 March 2018, https://plus.maths.org/content/cosmic-oracle-2#:~:text=In%20the%20power%20spectrum%20of,to%20regions%20at%20minimal%20density.
[49] Zhao, Y. "*CMB Foreground and separation methods.*" 12 May 2018, http://background.uchicago.edu/~whu/Courses/Ast448_18/zhao.pdf.
[50] Hilton, M., et. al., *THE ATACAMA COSMOLOGY TELESCOPE: THE TWO-SEASON ACTPOL SUNYAEV-ZEL'DOVICH EFFECT SELECTED CLUSTER CATALOG*, (2018), arXiv: 1709.05600v2
[51] Huang, C. C., "*The Discrete Fourier Transform.*" http://www.wright.edu/~chaocheng.huang/lecture/mth6060/6060chap4.pdf. Accessed 12 August 2023.
[52] "*Introduction*." Atacama Cosmology Telescope, https://act.princeton.edu/overview. Accessed 12 August 2023.
[53] "*The sky as seen by Planck*." ESA, 17 July 2018, https://sci.esa.int/web/planck/-/60503-the-sky-as-seen-by-planck.
[54] Atkins, Z., et. al., *The Atacama Cosmology Telescope: Map-Based Noise Simulations for DR6*, (2023), arXiv: 2303.04180
[55] Liu, H., et. al., *E and B families of the Stokes parameters in the polarized synchrotron and thermal dust foregrounds*, (2018), arXiv: 1804.10382v3